

# Nanoscale coherent intergrowths in a crystal of $\text{La}_{1.9}\text{Ca}_{1.1}\text{Cu}_2\text{O}_{6+\delta}$ made superconducting by high-pressure oxygen annealing

Hefei Hu,<sup>1</sup> Yimei Zhu,<sup>1</sup> Xiaoya Shi,<sup>1</sup> Qiang Li,<sup>1</sup> Ruidan Zhong,<sup>1</sup> John A. Schneeloch,<sup>1</sup> Genda Gu,<sup>1</sup> John M. Tranquada,<sup>1</sup> and Simon J. L. Billinge<sup>1,2,\*</sup>

<sup>1</sup>*Condensed Matter Physics and Materials Science Department,  
Brookhaven National Laboratory, Upton, New York 11973, USA*

<sup>2</sup>*Department of Applied Physics and Applied Mathematics,  
Columbia University, New York, NY 10027, USA*

(Dated: August 25, 2014)

Superconductivity with  $T_c = 53.5$  K has been induced in a large  $\text{La}_{1.9}\text{Ca}_{1.1}\text{Cu}_2\text{O}_6$  (La-2126) single crystal by annealing in a high partial-pressure of oxygen at 1200°C. Using transmission electron microscopy (TEM) techniques, we show that a secondary Ca-doped  $\text{La}_2\text{CuO}_4$  (La-214) phase, not present in the as-grown crystal, appears as a coherent “intergrowth” as a consequence of the annealing. A corresponding secondary superconducting transition near 13 K is evident in the magnetization measurement. Electron energy loss spectroscopy (EELS) reveals a pre-edge peak at the O  $K$  edge in the superconducting La-2126 phase, which is absent in the as-grown crystal, confirming the hole-doping by interstitial oxygen.

PACS numbers: 74.72.-h, 74.72.Gh, 68.37.-d, 79.20.Uv

## I. INTRODUCTION

$\text{La}_{1.9}\text{Ca}_{1.1}\text{Cu}_2\text{O}_6$ , abbreviated as La-2126,<sup>1</sup> is closely related to the canonical high-temperature superconductor  $\text{La}_{2-x}\text{A}_x\text{CuO}_4$  (where  $A$  is an alkaline earth element such as Ca, Sr or Ba) but with double, rather than single,  $\text{CuO}_2$  layers. Similar to  $\text{YBa}_2\text{Cu}_3\text{O}_{7-\delta}$  (YBCO), the structure has double  $\text{CuO}_2$  pyramidal layers separated by Ca rather than Y, and it has no CuO chains. This simple bilayer structure offers some advantages for studying the mechanism of superconductivity in the cuprates; however, synthesis of good superconducting La-2126 is challenging because of the required high-pressure-oxygen treatment.<sup>2-7</sup> So far, investigations of the atomic and electronic structure of La-2126 have been limited, as the superconducting samples are generally polycrystalline.

Here we report the characterization of a large La-2126 crystal in which superconductivity has been induced by high-pressure annealing in oxygen. In particular, we have used transmission electron microscopy (TEM) techniques to compare the structure of superconducting crystals with the as-grown, nonsuperconducting starting material. While the nonsuperconducting samples are found to be structurally homogenous, a minority phase of  $\text{La}_{2-x}\text{Ca}_x\text{CuO}_4$  (La-214) is directly detected in superconducting samples by electron diffraction as well as high-angle annular dark-field (HAADF) imaging (also called Z-contrast imaging) and electron energy-loss spectroscopy (EELS) in scanning transmission electron microscopy (STEM) mode. Layers of the La-214 phase are found to be coherently interspersed along the  $c$ -axis direction of the primary La-2126 phase. The energy-loss near-edge structure (ELNES) measured at the O  $K$  edge on the primary La-2126 phase in the superconducting sample shows a pre-edge peak that is absent for the non-superconducting sample. The presence of the pre-edge

peak reflects the doping effect of the interstitial oxygens introduced by the high-pressure annealing. While the occurrence of the La-214 “intergrowths” does not seem to harm the superconductivity of the La-2126 phase, it nevertheless appears to have an associated superconducting transition at  $\sim 13$  K, as evidenced by magnetization measurements.

## II. EXPERIMENT

Single crystals of La-2126 were grown in a floating-zone furnace equipped with two ellipsoidal mirrors.<sup>8</sup> The powders of  $\text{La}_2\text{O}_3$ ,  $\text{CaCO}_3$  and  $\text{CuO}$  (99.99%) in their metal ratio were mixed and ground in an agate mortar, and first calcined for 24h at 980°C. The calcined powders were then reground and calcined for 48h at 1050°C for feed rods. The powders were again reground and placed into a rubber tube, and then hydrostatically pressed. The pressed feed rods were sintered for 72h at 1100°C in air. After mounting in the floating-zone furnace with an oxygen atmosphere (pressure of 11 bars), the sintered feed rod was pre-melted at a travelling-zone velocity of 25 mm/h in order to increase the feed-rod density, which impacts the stability of the molten zone during crystal growth. The crystal rod was grown at a velocity of 0.4 mm/h under 11 bars of oxygen. Polished sections of the as-grown rod were examined by an optical polarization microscope to ensure the absence of secondary crystal domains. The composition of the rods was analyzed by electron probe micro-analyzer (EPMA) on the polished cross sections. The quality of single-crystal rods was confirmed by neutron diffraction.<sup>9</sup>

The as-grown rod was not superconducting. To induce bulk superconductivity, a crystal 8 mm in diameter and 10 mm in length was annealed in a hot isotstatic press, with a gas mixture of 20% oxygen and 80% argon at

a pressure of 7000 bar and temperature of 1200°C, for 10 hours, followed by cooling at the rate of 500°C per hour. We note that the high-pressure annealing temperature was above the atmospheric-pressure melting point ( $\sim 1120^\circ\text{C}$ ) of La-2126; however, the annealed crystal exhibited no external signs of melting or decomposition, indicating that the melting point under the high-pressure conditions is greater than 1200°C.

Characterizations were performed on pieces cut from the annealed and as-grown crystals. The magnetization measurements were carried out by using a superconducting quantum interference device (SQUID). All TEM-related experiments were performed using a JEOL ARM 200CF transmission electron microscope operated at 200 kV, which is equipped with double aberration correctors (CEOS) and a cold field-emission gun. The TEM samples were prepared by crushing the bulk material into thin flakes transparent to the electron beam, which were then placed on a copper grid coated with a lacey carbon film.

### III. CHARACTERIZATION RESULTS

Figure 1 shows the magnetization measurement of a piece cut from the oxygen-treated superconducting La-2126 sample at a magnetic field  $H$  of 2 Oe parallel to the  $c$  axis.  $T_c$  was determined to be 53.5 K by linearly extrapolating the  $4\pi M$  data at superconducting transition to the zero magnetization line. Interestingly, a small drop is observed at  $\sim 13$  K, implying the presence of a secondary superconducting phase. The zero-field-cooled (ZFC) measurement indicates nearly full shielding below the sharp high-temperature transition; the low-temperature transition has only a weak effect on the shielding fraction. The Meissner fraction, determined by the FC measurement, is small, but this is not uncommon

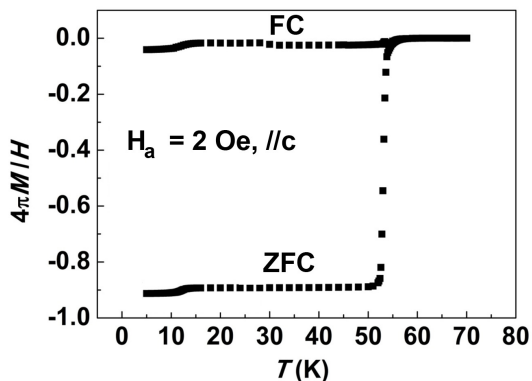


FIG. 1: Temperature-dependent magnetic susceptibility ( $M/H$ ) of superconducting  $\text{La}_{1.9}\text{Ca}_{1.1}\text{Cu}_2\text{O}_{6+\delta}$  single crystal, measured at 2 Oe externally applied magnetic field. Measurements were performed both in zero-field cooling (ZFC) and field-cooling (FC) modes. Magnetic field is parallel to the  $c$ -axis of the crystal.

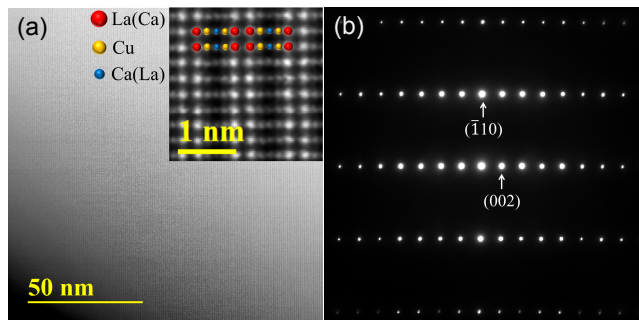


FIG. 2: (a) ADF image along  $[110]$  of the as-grown nonsuperconducting sample. The inset shows the atomic-resolution image. (b) Electron diffraction from the area shown in (a).

for cuprates. (Small observed Meissner fractions are frequently attributed to flux pinning on cooling through  $T_c$ .)

Figure 2(a) shows a representative HAADF-STEM image of the as-grown sample, viewed down the  $[110]$  zone axis at medium magnification. The contrast gradient is due to variation in the sample thickness. A typical atomic-resolution HAADF image is shown in the insert. Only heavy atoms are shown in the structure model, since oxygen is too light to be seen in the HAADF-STEM image next to the heavier metal atoms. From x-ray<sup>1</sup> and neutron<sup>10</sup> diffraction studies of  $\text{La}_{1.9}\text{Ca}_{1.1}\text{Cu}_2\text{O}_6$ , the La and Ca are known to have preferred sites, but with substitutional disorder. Within the  $I4/mmm$  space group, La dominates the  $4e$  sites with  $\sim 90\%$  occupancy, while Ca prefers the  $2a$  sites, with a similar average occupancy<sup>1,10</sup>; in the atomic-resolution inset of Fig. 2(a), these atoms are denoted by the largest (red) and smallest (blue) circles, respectively. Figure 2(b) shows the electron diffraction pattern from the same area as in (a). Some of the diffraction spots are indexed. Overall, the as-grown samples show good structural homogeneity.

The superconducting samples prepared by the high-pressure-oxygen treatment were studied next. Figure 3(a) shows a representative HAADF-STEM image of the oxygen-annealed sample down the same  $[110]$  zone axis. Surprisingly, stripes with high contrast are clearly evident. A typical atomic-resolution HAADF image, as seen in Fig. 3(b), shows that an “intergrowth” phase has formed, which contributes to the high contrast seen in Fig. 3(a). This new phase demonstrates coherent interfaces with the primary La-2126 phase, indicating a similar lattice constant  $a$  for these two phases. The new phase was identified as  $\text{La}_{2-x}\text{Ca}_x\text{CuO}_4$  (La-214), from a combination of the measured lattice constant  $c$  and analysis of the chemical composition (see below). La-214 has higher mass density than La-2126, resulting in a higher contrast in the Z-contrast HAADF-STEM images. It is noted that tetragonal phases ( $I4/mmm$ ) of La-214 ( $a = 3.801 \text{ \AA}$ ,  $c = 13.23 \text{ \AA}$  for  $x = 0.1$ )<sup>11</sup> and La-2126 ( $a = 3.825 \text{ \AA}$ ,  $c = 19.41 \text{ \AA}$ )<sup>1,10</sup> have lattice constants  $a$  that differ by only  $\sim 0.6\%$ , resulting in coherent interfaces (Fig. 3(b)). The lattice constant  $c$  of La-214 is approximately  $\frac{2}{3}$  of

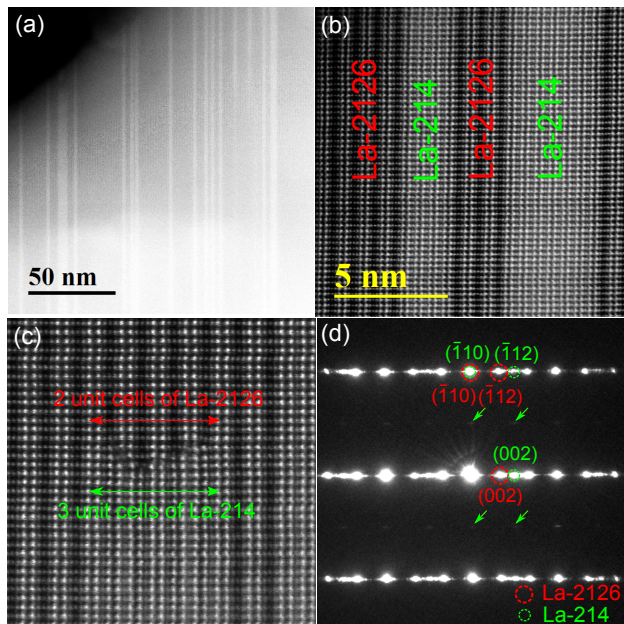


FIG. 3: (a) ADF image along  $[110]$  of the superconducting sample after post high-pressure oxygen treatment. (b) and (c) Atomic-resolution image expanded from the region shown in (a). Green and red labels indicate the different materials. (c) illustrates the lattice modulating between La-2126 and La-214 that allows for the intergrowth. (d) Electron diffraction from the area shown in (a). Some reflections are labeled for La2126 and La214 phases, respectively.

that of La-2126, which allows for another commensurability: 3 layers of La-214 can replace 2 layers of La-2126, with little strain on the surrounding lattice. This pattern can be seen in Fig. 3(c) where the width of the La-214 “intergrowths” is typically an integral multiple of 3 unit cells along the  $c$  axis. In our STEM images, most La-214 domains are 3-unit-cells wide, while 6- and 9-unit-cell wide domains are also observed (Fig. 3(a)). Rarely, a 1.5-unit-cell width of La-214 can also occur, corresponding to one unit cell of La-2126. This is possible because a single unit cell of La-214 contains two  $\text{CuO}_2$  planes, so that 1.5 unit cells corresponds to 3  $\text{CuO}_2$  layers. Figure 3(d) shows the corresponding electron diffraction pattern with some reflections indexed for La-2126 and La-214, respectively. It is noted that all of the reflections are broadened along  $c^*$ , which results from the random spacing of the intergrowths along the  $c$ -axis.

We next probed the elemental distribution across the intergrowths using atomic-resolution line scan EELS. A typical EELS spectrum recorded from a large area containing both La-2126 and La-214 phases is shown in Fig. 4(a) with  $\text{Ca-}L_{2,3}$ ,  $\text{O-}K$  and  $\text{La-}M_{4,5}$  edges, with increasing energy. Figure 4(b) shows an atomic-resolution HAADF image with a scan path running from La-2126 to La-214. EELS spectra were recorded along this scan path with an interval of 0.5 Å. After removal of background with a power-law function, intensity of  $\text{La-}M_{4,5}$  and  $\text{Ca-}$

$L_{2,3}$  edges were integrated for each spectrum along the scan path, and plotted as a function of scan position as shown in Fig. 4(c) and Fig. 4(d), respectively. The eight peaks in the  $\text{La-}M_{4,5}$  intensity profile correspond to the eight bright La atomic columns, with the first two from the La-2126 and the rest from the La-214. The  $\text{Ca-}L_{2,3}$  intensity profile shows two sharp peaks corresponding to two Ca atomic columns in the La-2126. Ca atoms in La-214 share sites with La. The Ca signal does not drop to zero but also shows no clear modulation, indicating that the concentration of Ca in the La-214 is fairly small, compared to that in La-2126, as expected. When La-214 is grown in air, the solubility limit of Ca is  $x \sim 0.1$ ; however, this can be raised to 0.2 by use of high-pressure oxygen.<sup>12</sup> We are not able to precisely determine the Ca (or possible excess O) concentration in the intergrowth phase. In any case, it seems likely that the La-214 intergrowths are associated with the small increase in the diamagnetic susceptibility around 13 K seen in Fig. 1.

From the magnetization measurement, it is noted that La-2126 is still the primary phase contributing to superconductivity in the sample. To investigate how oxygen incorporation impacts the electronic structure of the sample,  $\text{O-}K$  ELNES data, recorded in STEM mode from the as-grown non-superconducting sample and the matrix La-2126 of the superconducting sample, respectively, were compared. The electron probe was intentionally defocused and kept scanning over the area of interest to avoid beam damage. Beam current and acquisition time were also optimized to ensure good statistics and no noticeable damage. The background removed  $\text{O-}K$  ELNES are plotted in black for the nonsuperconducting sample and in red for the superconducting sample, as shown in Fig. 5; each curve has been normalized to its maximum intensity to allow meaningful comparison. There are 5 distinct features seen in the fine structures, which are labeled as  $a$ ,  $b$ ,  $c$ ,  $d$  and  $e$ , respectively. Peaks  $b$ ,  $c$ ,  $d$  and  $e$  show little or no difference between the two samples. The main difference is the appearance of pre-edge peak  $a$  in the superconducting sample, which corresponds to excitations from the  $\text{O } 1s$  level into  $\text{O } 2p$  holes.<sup>13,14</sup> It steals weight from the peak at  $\sim 1$  eV higher energy, present in the nonsuperconducting sample, which is associated with excitations into a  $\text{Cu } 3d$  hole on a neighboring site via hybridization with  $\text{O } 2p$  states. The absence of the pre-edge peak in the nonsuperconducting sample is consistent with neutron diffraction evidence for antiferromagnetic order.<sup>9</sup> The presence of the  $\text{O } 2p$  holes in the superconducting sample provides indirect evidence for intercalated oxygen, which is necessary to pull electrons out of the  $\text{CuO}_2$  planes.

#### IV. DISCUSSION AND CONCLUSIONS

The detection of 214 layers interspersed in the La-2126 lattice came as a surprise, given the relatively high  $T_c$  and sharp transition of the annealed crystal. Given that the

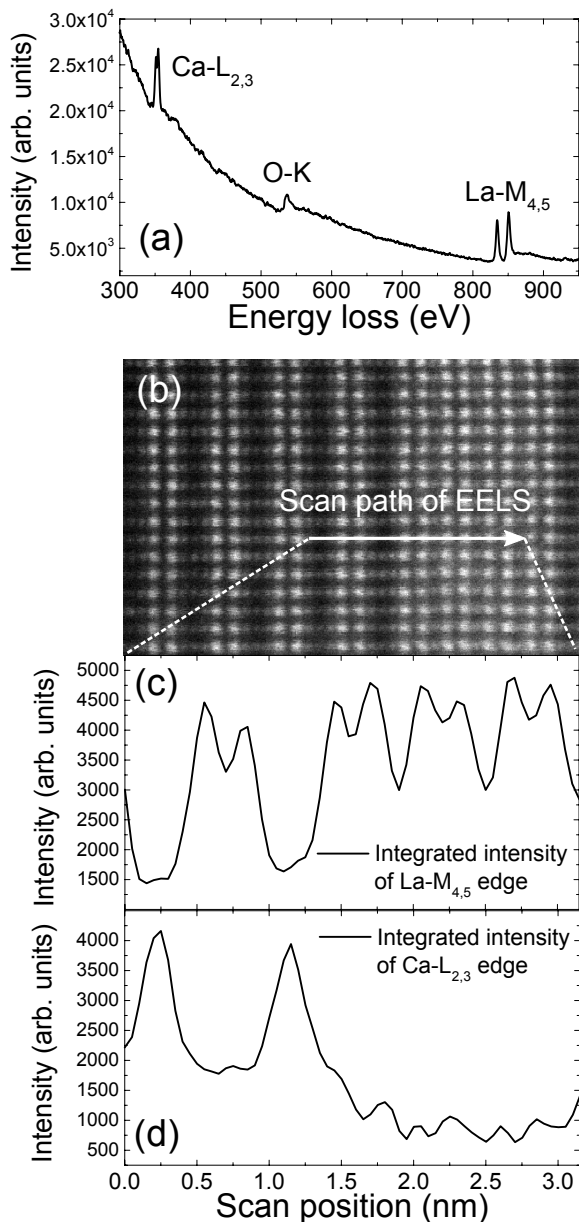


FIG. 4: A typical EELS spectrum (a) and atomic resolution image (b) from the superconducting oxygen-annealed sample. Integrated intensity of (c) La- $M_{4,5}$  and (d) Ca- $L_{2,3}$  edge features shown in (a) along the scan path shown in (b).

starting material is pure, homogeneous La-2126, the development of the 214 layers must involve the transformation of La-2126 layers; as such, it is inaccurate to characterize the 214 layers as intergrowths. To accomplish the transformation from La-2126 to 214, some CaO and CuO must be removed. As such phases have not been detected by TEM, we suspect that they diffused out of the

sample at the high annealing temperature. Presumably, such a decomposition can be reduced or eliminated by annealing at lower temperatures. Now that we have established that high-pressure oxygen annealing can transform as-grown La-2126 crystals to bulk superconductors,

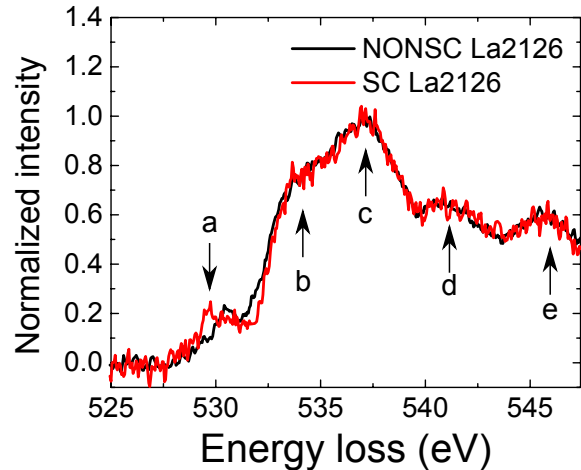


FIG. 5: Comparison of O-K edge fine structures between the as-grown nonsuperconducting sample (black) and the remaining La-2126 of the superconducting sample after oxygen treatment (red).

we have strong motivation to explore reduced annealing temperature in future work.

In summary, we synthesized single crystals of superconducting La-2126 with  $T_c \sim 53.5$  K by using high-pressure-oxygen annealing. The changes in both atomic and electronic structures of La-2126 were investigated after the high-oxygen-pressure treatment. A secondary Ca-doped La-214 phase intergrown with La-2126 has been directly detected, and it appears to be associated with a second superconducting transition at around 13 K indicated by the magnetization measurement. Measurements of O-K ELNES are consistent with the non-superconducting sample being a correlated insulator, while O  $2p$  holes are present in the superconducting sample.

### Acknowledgments

This work was carried out as part of the FlucTeam project at Brookhaven National Laboratory, supported by the US Department of Energy, Office of Science, Office of Basic Energy Sciences (DOE-BES) through account DE-AC02-98CH10886. R.D.Z. and J.A.S. are supported by the Center for Emergent Superconductivity, an Energy Frontier Research Center. We thank K. Mohanty and E. Stein for performing the high-pressure annealing.

\* Electronic address: [billinge@bnl.gov](mailto:billinge@bnl.gov)

<sup>1</sup> N. Nguyen, L. Er-Rakho, C. Michel, J. Choynet, and

- B. Raveau, *Mater. Res. Bull.* **15**, 891 (1980).
- <sup>2</sup> R. J. Cava, B. Batlogg, R. B. van Dover, J. J. Krajewski, J. V. Waszczak, R. M. Fleming, W. F. Peck, L. W. Rupp, P. Marsh, A. C. W. P. James, et al., *Nature* **345**, 602 (1990).
- <sup>3</sup> K. Kinoshita, H. Shibata, and T. Yamada, *Jpn. J. Appl. Phys.* **29**, L1632 (1990).
- <sup>4</sup> K. Kinoshita, H. Shibata, and T. Yamada, *Physica C* **171**, 523 (1990).
- <sup>5</sup> T. Ishii, T. Watanabe, K. Kinoshita, and A. Matsuda, *Physica C* **179**, 39 (1991).
- <sup>6</sup> T. Watanabe, K. Kinoshita, and A. Matsuda, *Phys. Rev. B* **47**, 11544 (1993).
- <sup>7</sup> M. Okuya, T. Kimura, R. Kobayashi, J. Shimoyama, K. Kitazawa, K. Yamafuji, K. Kishio, K. Kinoshita, and T. Yamada, *J. Supercond.* **7**, 313 (1994).
- <sup>8</sup> G. Gu, M. Hücker, Y.-J. Kim, J. Tranquada, Q. Li, and A. Moodenbaugh, *J. Cryst. Growth.* **287**, 318 (2006).
- <sup>9</sup> M. Hücker, Y.-J. Kim, G. D. Gu, J. M. Tranquada, B. D. Gaulin, and J. W. Lynn, *Phys. Rev. B* **71**, 094510 (2005).
- <sup>10</sup> F. Izumi, E. Takayama-Muromachi, Y. Nakai, and H. Asano, *Physica C* **157**, 89 (1989).
- <sup>11</sup> A. N. Christensen and B. Lebech, *Acta Chem. Scand.* **44**, 902 (1990).
- <sup>12</sup> B. Dabrowski, Z. Wang, K. Rogacki, J. D. Jorgensen, R. L. Hitterman, J. L. Wagner, B. A. Hunter, P. G. Radaelli, and D. G. Hinks, *Phys. Rev. Lett.* **76**, 1348 (1996).
- <sup>13</sup> C. T. Chen, F. Sette, Y. Ma, M. S. Hybertsen, E. B. Stechel, W. M. C. Foulkes, M. Schulter, S.-W. Cheong, A. S. Cooper, L. W. Rupp, et al., *Phys. Rev. Lett.* **66**, 104 (1991).
- <sup>14</sup> J. Fink, N. Nücker, E. Pellegrin, H. Romberg, M. Alexander, and M. Knupfer, *J. Electron Spec. Related Phenomena* **66**, 395 (1994).